

Diffractional Photoproduction of $\psi(2S)$ Mesons at HERA

H1 Collaboration

Abstract

Results on diffractive photoproduction of $\psi(2S)$ mesons are presented using data collected between 1996 and 2000 with the H1 detector at the HERA ep collider. The data correspond to an integrated luminosity of 77 pb^{-1} . The energy dependence of the diffractive $\psi(2S)$ cross section is found to be similar to or possibly somewhat steeper than that for J/ψ mesons. The dependences of the elastic and proton dissociative $\psi(2S)$ photoproduction cross sections on the squared momentum transfer t at the proton vertex are measured. The t -dependence of the elastic channel, parametrised as e^{bt} , yields $b_{el}^{\psi(2S)} = (4.31 \pm 0.57 \pm 0.46) \text{ GeV}^{-2}$, compatible with that of the J/ψ . For the proton dissociative channel the result $b_{pd}^{\psi(2S)} = (0.59 \pm 0.13 \pm 0.12) \text{ GeV}^{-2}$ is 2.3 standard deviations smaller than that measured for the J/ψ . With proper account of the individual wavefunctions theoretical predictions based on perturbative QCD are found to describe the measurements well.

To be submitted to Phys. Lett. B

C. Adloff³³, V. Andreev²⁴, B. Andrieu²⁷, T. Anthonis⁴, A. Astvatsatourov³⁵, A. Babaev²³,
 J. Bähr³⁵, P. Baranov²⁴, E. Barrelet²⁸, W. Bartel¹⁰, S. Baumgartner³⁶, J. Becker³⁷,
 M. Beckingham²¹, A. Beglarian³⁴, O. Behnke¹³, C. Beier¹⁴, A. Belousov²⁴, Ch. Berger¹,
 T. Berndt¹⁴, J.C. Bizot²⁶, J. Böhme¹⁰, V. Boudry²⁷, W. Braunschweig¹, V. Brisson²⁶,
 H.-B. Bröker², D.P. Brown¹⁰, W. Brückner¹², D. Bruncko¹⁶, F.W. Büsler¹¹, A. Bunyatyan^{12,34},
 A. Burrage¹⁸, G. Buschhorn²⁵, L. Bystritskaya²³, A.J. Campbell¹⁰, S. Caron¹,
 F. Cassol-Brunner²², D. Clarke⁵, C. Collard⁴, J.G. Contreras^{7,41}, Y.R. Coppens³,
 J.A. Coughlan⁵, M.-C. Cousinou²², B.E. Cox²¹, G. Cozzika⁹, J. Cvach²⁹, J.B. Dainton¹⁸,
 W.D. Dau¹⁵, K. Daum^{33,39}, M. Davidsson²⁰, B. Delcourt²⁶, N. Delerue²², R. Demirchyan³⁴,
 A. De Roeck^{10,43}, E.A. De Wolf⁴, C. Diaconu²², J. Dingfelder¹³, P. Dixon¹⁹, V. Dodonov¹²,
 J.D. Dowell³, A. Drouskoi²³, A. Dubak²⁵, C. Duprel², G. Eckerlin¹⁰, D. Eckstein³⁵,
 V. Efremenko²³, S. Egli³², R. Eichler³⁶, F. Eisele¹³, E. Eisenhandler¹⁹, M. Ellerbrock¹³,
 E. Elsen¹⁰, M. Erdmann^{10,40,e}, W. Erdmann³⁶, P.J.W. Faulkner³, L. Favart⁴, A. Fedotov²³,
 R. Felst¹⁰, J. Ferencei¹⁰, S. Ferron²⁷, M. Fleischer¹⁰, P. Fleischmann¹⁰, Y.H. Fleming³,
 G. Flügge², A. Fomenko²⁴, I. Foresti³⁷, J. Formánek³⁰, G. Franke¹⁰, G. Frising¹,
 E. Gabathuler¹⁸, K. Gabathuler³², J. Garvey³, J. Gassner³², J. Gayler¹⁰, R. Gerhards¹⁰,
 C. Gerlich¹³, S. Ghazaryan^{4,34}, L. Goerlich⁶, N. Gogitidze²⁴, C. Grab³⁶, V. Grabski³⁴,
 H. Grässler², T. Greenshaw¹⁸, G. Grindhammer²⁵, T. Hadig¹³, D. Haidt¹⁰, L. Hajduk⁶,
 J. Haller¹³, W.J. Haynes⁵, B. Heinemann¹⁸, G. Heinzelmann¹¹, R.C.W. Henderson¹⁷,
 S. Hengstmann³⁷, H. Henschel³⁵, R. Heremans⁴, G. Herrera^{7,44}, I. Herynek²⁹,
 M. Hildebrandt³⁷, M. Hilgers³⁶, K.H. Hiller³⁵, J. Hladký²⁹, P. Höting², D. Hoffmann²²,
 R. Horisberger³², A. Hovhannisyanyan³⁴, S. Hurling¹⁰, M. Ibbotson²¹, Ç. İşsever⁷, M. Jacquet²⁶,
 M. Jaffre²⁶, L. Janauschek²⁵, X. Janssen⁴, V. Jemanov¹¹, L. Jönsson²⁰, C. Johnson³,
 D.P. Johnson⁴, M.A.S. Jones¹⁸, H. Jung^{20,10}, D. Kant¹⁹, M. Kapichine⁸, M. Karlsson²⁰,
 O. Karschnick¹¹, F. Keil¹⁴, N. Keller³⁷, J. Kennedy¹⁸, I.R. Kenyon³, S. Kermiche²²,
 C. Kiesling²⁵, P. Kjellberg²⁰, M. Klein³⁵, C. Kleinwort¹⁰, T. Kluge¹, G. Knies¹⁰, B. Koblitz²⁵,
 S.D. Kolya²¹, V. Korbel¹⁰, P. Kostka³⁵, S.K. Kotelnikov²⁴, R. Koutouev¹², A. Koutov⁸,
 J. Kroseberg³⁷, K. Krüger¹⁰, T. Kuhr¹¹, T. Kurča¹⁶, D. Lamb³, M.P.J. Landon¹⁹, W. Lange³⁵,
 T. Laštovička^{35,30}, P. Laycock¹⁸, E. Lebailly²⁶, A. Lebedev²⁴, B. Leißner¹, R. Lemrani¹⁰,
 V. Lendermann⁷, S. Levonian¹⁰, M. Lindstroem²⁰, B. List³⁶, E. Lobodzinska^{10,6},
 B. Lobodzinski^{6,10}, A. Loginov²³, N. Loktionova²⁴, V. Lubimov²³, S. Lüders³⁶, D. Lüke^{7,10},
 L. Lytkin¹², N. Malden²¹, E. Malinovski²⁴, I. Malinovski²⁴, S. Mangano³⁶, R. Maraček²⁵,
 P. Marage⁴, J. Marks¹³, R. Marshall²¹, H.-U. Martyn¹, J. Martyniak⁶, S.J. Maxfield¹⁸,
 D. Meer³⁶, A. Mehta¹⁸, K. Meier¹⁴, A.B. Meyer¹¹, H. Meyer³³, J. Meyer¹⁰, P.-O. Meyer²,
 S. Mikocki⁶, D. Milstead¹⁸, S. Mohr dieck¹¹, M.N. Mondragon⁷, F. Moreau²⁷, A. Morozov⁸,
 J.V. Morris⁵, K. Müller³⁷, P. Murín^{16,42}, V. Nagovizin²³, B. Naroska¹¹, J. Naumann⁷,
 Th. Naumann³⁵, G. Nellen²⁵, P.R. Newman³, F. Niebergall¹¹, C. Niebuhr¹⁰, O. Nix¹⁴,
 G. Nowak⁶, J.E. Olsson¹⁰, D. Ozerov²³, V. Panassik⁸, C. Pascaud²⁶, G.D. Patel¹⁸, M. Peez²²,
 E. Perez⁹, A. Petrukhin³⁵, J.P. Phillips¹⁸, D. Pitzl¹⁰, R. Pöschl²⁶, I. Potachnikova¹², B. Povh¹²,
 G. Rädcl¹, J. Rauschenberger¹¹, P. Reimer²⁹, B. Reisert²⁵, C. Risler²⁵, E. Rizvi³,
 P. Robmann³⁷, R. Roosen⁴, A. Rostovtsev²³, S. Rusakov²⁴, K. Rybicki⁶, J. Samson³⁶,
 D.P.C. Sankey⁵, S. Schätzel¹³, J. Scheins¹, F.-P. Schilling¹⁰, P. Schleper¹⁰, D. Schmidt³³,
 D. Schmidt¹⁰, S. Schmidt²⁵, S. Schmitt¹⁰, M. Schneider²², L. Schoeffel⁹, A. Schöning³⁶,
 T. Schörner²⁵, V. Schröder¹⁰, H.-C. Schultz-Coulon⁷, C. Schwanenberger¹⁰, K. Sedlák²⁹,
 F. Sefkow³⁷, V. Shekelyan²⁵, I. Sheviakov²⁴, L.N. Shtarkov²⁴, Y. Sirois²⁷, T. Sloan¹⁷,
 P. Smirnov²⁴, Y. Soloviev²⁴, D. South²¹, V. Spaskov⁸, A. Specka²⁷, H. Spitzer¹¹, R. Stamen⁷,

B. Stella³¹, J. Stiewe¹⁴, I. Strauch¹⁰, U. Straumann³⁷, M. Swart¹⁴, S. Tchetchelnitski²³, G. Thompson¹⁹, P.D. Thompson³, F. Tomasz¹⁴, D. Traynor¹⁹, P. Truöl³⁷, G. Tsipolitis^{10,38}, I. Tsurin³⁵, J. Turnau⁶, J.E. Turney¹⁹, E. Tzamariudaki²⁵, S. Udluft²⁵, A. Uraev²³, M. Urban³⁷, A. Usik²⁴, S. Valkár³⁰, A. Valkárová³⁰, C. Vallée²², P. Van Mechelen⁴, S. Vassiliev⁸, Y. Vazdik²⁴, A. Vest¹, A. Vichnevski⁸, K. Wacker⁷, J. Wagner¹⁰, R. Wallny³⁷, B. Waugh²¹, G. Weber¹¹, D. Wegener⁷, C. Werner¹³, N. Werner³⁷, M. Wessels¹, G. White¹⁷, S. Wiesand³³, T. Wilksen¹⁰, M. Winde³⁵, G.-G. Winter¹⁰, Ch. Wissing⁷, M. Wobisch¹⁰, E.-E. Woehrling³, E. Wunsch¹⁰, A.C. Wyatt²¹, J. Žáček³⁰, J. Zálešák³⁰, Z. Zhang²⁶, A. Zhokin²³, F. Zomer²⁶, and M. zur Nedden¹⁰

¹ *I. Physikalisches Institut der RWTH, Aachen, Germany^a*

² *III. Physikalisches Institut der RWTH, Aachen, Germany^a*

³ *School of Physics and Space Research, University of Birmingham, Birmingham, UK^b*

⁴ *Inter-University Institute for High Energies ULB-VUB, Brussels; Universiteit Antwerpen (UIA), Antwerpen; Belgium^c*

⁵ *Rutherford Appleton Laboratory, Chilton, Didcot, UK^b*

⁶ *Institute for Nuclear Physics, Cracow, Poland^d*

⁷ *Institut für Physik, Universität Dortmund, Dortmund, Germany^a*

⁸ *Joint Institute for Nuclear Research, Dubna, Russia*

⁹ *CEA, DSM/DAPNIA, CE-Saclay, Gif-sur-Yvette, France*

¹⁰ *DESY, Hamburg, Germany*

¹¹ *Institut für Experimentalphysik, Universität Hamburg, Hamburg, Germany^a*

¹² *Max-Planck-Institut für Kernphysik, Heidelberg, Germany*

¹³ *Physikalisches Institut, Universität Heidelberg, Heidelberg, Germany^a*

¹⁴ *Kirchhoff-Institut für Physik, Universität Heidelberg, Heidelberg, Germany^a*

¹⁵ *Institut für experimentelle und Angewandte Physik, Universität Kiel, Kiel, Germany*

¹⁶ *Institute of Experimental Physics, Slovak Academy of Sciences, Košice, Slovak Republic^{e,f}*

¹⁷ *School of Physics and Chemistry, University of Lancaster, Lancaster, UK^b*

¹⁸ *Department of Physics, University of Liverpool, Liverpool, UK^b*

¹⁹ *Queen Mary and Westfield College, London, UK^b*

²⁰ *Physics Department, University of Lund, Lund, Sweden^g*

²¹ *Physics Department, University of Manchester, Manchester, UK^b*

²² *CPPM, CNRS/IN2P3 - Univ Méditerranée, Marseille - France*

²³ *Institute for Theoretical and Experimental Physics, Moscow, Russia^l*

²⁴ *Lebedev Physical Institute, Moscow, Russia^e*

²⁵ *Max-Planck-Institut für Physik, München, Germany*

²⁶ *LAL, Université de Paris-Sud, IN2P3-CNRS, Orsay, France*

²⁷ *LPNHE, Ecole Polytechnique, IN2P3-CNRS, Palaiseau, France*

²⁸ *LPNHE, Universités Paris VI and VII, IN2P3-CNRS, Paris, France*

²⁹ *Institute of Physics, Academy of Sciences of the Czech Republic, Praha, Czech Republic^{e,i}*

³⁰ *Faculty of Mathematics and Physics, Charles University, Praha, Czech Republic^{e,i}*

³¹ *Dipartimento di Fisica Università di Roma Tre and INFN Roma 3, Roma, Italy*

³² *Paul Scherrer Institut, Villigen, Switzerland*

³³ *Fachbereich Physik, Bergische Universität Gesamthochschule Wuppertal, Wuppertal, Germany*

³⁴ *Yerevan Physics Institute, Yerevan, Armenia*

³⁵ *DESY, Zeuthen, Germany*

³⁶ *Institut für Teilchenphysik, ETH, Zürich, Switzerland^j*

³⁷ *Physik-Institut der Universität Zürich, Zürich, Switzerland^j*

³⁸ *Also at Physics Department, National Technical University, Zografou Campus, GR-15773 Athens, Greece*

³⁹ *Also at Rechenzentrum, Bergische Universität Gesamthochschule Wuppertal, Germany*

⁴⁰ *Also at Institut für Experimentelle Kernphysik, Universität Karlsruhe, Karlsruhe, Germany*

⁴¹ *Also at Dept. Fis. Ap. CINVESTAV, Mérida, Yucatán, México^k*

⁴² *Also at University of P.J. Šafárik, Košice, Slovak Republic*

⁴³ *Also at CERN, Geneva, Switzerland*

⁴⁴ *Also at Dept. Fis. CINVESTAV, México City, México^k*

^a *Supported by the Bundesministerium für Bildung und Forschung, FRG, under contract numbers 05 H1 1GUA /1, 05 H1 1PAA /1, 05 H1 1PAB /9, 05 H1 1PEA /6, 05 H1 1VHA /7 and 05 H1 1VHB /5*

^b *Supported by the UK Particle Physics and Astronomy Research Council, and formerly by the UK Science and Engineering Research Council*

^c *Supported by FNRS-FWO-Vlaanderen, IISN-IKW and IWT*

^d *Partially Supported by the Polish State Committee for Scientific Research, grant no. 2P0310318 and SPUB/DESY/P03/DZ-1/99 and by the German Bundesministerium für Bildung und Forschung*

^e *Supported by the Deutsche Forschungsgemeinschaft*

^f *Supported by VEGA SR grant no. 2/1169/2001*

^g *Supported by the Swedish Natural Science Research Council*

ⁱ *Supported by the Ministry of Education of the Czech Republic under the projects INGO-LA116/2000 and LN00A006 and by GAUK grant no 173/2000*

^j *Supported by the Swiss National Science Foundation*

^k *Supported by CONACyT*

^l *Partially Supported by Russian Foundation for Basic Research, grant no. 00-15-96584*

1 Introduction

We report on a measurement of diffractive photoproduction of $\psi(2S)$ mesons, $\gamma p \rightarrow \psi(2S) + Y$, where Y denotes either a proton or a proton dissociation system of mass $M_Y > m_p$. The data were taken with the H1 Detector at the ep collider HERA. The dependences of the cross section on $W_{\gamma p}$, the photon-proton center of mass energy, and on t , the square of the four-momentum transfer at the proton vertex, are measured for the first time and are compared to those of J/ψ production. The data cover the region $40 < W_{\gamma p} < 150$ GeV.

In recent years diffractive production of J/ψ mesons has been measured at HERA with increasing precision [1–4]. The cross section for the elastic process $\gamma p \rightarrow J/\psi p$ was found to rise steeply with $W_{\gamma p}$. This was interpreted as a signature for a “hard” process and calculations in perturbative Quantum Chromodynamics (pQCD) were able to give a good description of the data [5, 6]. In perturbative QCD, diffractive charmonium production in γp scattering can be viewed in the proton rest frame as a sequence of several steps separated in time. An almost real photon is emitted from the incoming lepton and fluctuates into a $c\bar{c}$ pair. The $c\bar{c}$ pair subsequently interacts with the proton via the exchange of two gluons (or a gluon ladder) in a colour-singlet state and then evolves into a real vector meson. In such models, with the $c\bar{c}$ fluctuation of the photon treated as a colour dipole, a number of distinct predictions are made for $\psi(2S)$ photoproduction [7–11]. The cross section for $\psi(2S)$ should be suppressed with respect to that for J/ψ , the dependence on $W_{\gamma p}$ should be somewhat steeper than that of the J/ψ photoproduction cross section and the t -dependence of $\psi(2S)$ production should be similar or somewhat shallower than that of J/ψ production. These predictions take into account the $\psi(2S)$ meson wavefunction which is different from that of the J/ψ meson in two respects. It has a larger expectation value for the radius than the ground state and it has a node (see e.g. [10]). The cross section for elastic $\psi(2S)$ production has been measured previously at HERA energies and the resulting ratio $\sigma_{\psi(2S)}/\sigma_{J/\psi} = 0.150 \pm 0.027(stat) \pm 0.018(syst) \pm 0.011(BR)$ [12] verifies the prediction of a suppression with respect to J/ψ production. This and the other predictions mentioned above are addressed in this paper.

In a geometric interpretation one expects the t -dependences, parametrised as $\propto e^{bt}$, to reflect the sizes of the interacting objects, similarly to the hadroproduction case. Vector mesons with large radii should have larger values of b than vector mesons with small radii. This has indeed been confirmed in photoproduction in the HERA energy range, where e.g. $b_{\rho^0} > b_{J/\psi}$ was measured [13, 14]. Since the radius of the $\psi(2S)$ meson is approximately a factor of two larger than that of the J/ψ meson one might naively expect a steeper t dependence. In QCD a different result is obtained. Due to cancellations in the contributions to the production amplitude from $c\bar{c}$ -quark dipoles with sizes above and below the node of the $\psi(2S)$ wavefunction, the t -dependence of elastic $\psi(2S)$ production has been predicted to be slightly shallower than that of the J/ψ meson [9].

Calculations of the t -dependences for light and heavy vector meson production also exist [15] using an additive quark model ansatz. These calculations are able to reproduce the measurements of the t -dependences at small $|t|$ for many elastic and proton dissociative processes.

2 Data Analysis

2.1 Kinematics

The kinematics of the process $ep \rightarrow e\psi Y$ are described by the following variables: the square of the ep center-of-mass energy $s = (p + k)^2$; the negative four-momentum transfer squared at the lepton vertex $Q^2 = -q^2 = -(k - k')^2$; the four-momentum transfer squared at the proton vertex $t = (p - p')^2$ and the scaled energy transfer $y = (p \cdot q)/(p \cdot k)$. The four-momenta k , k' , p , p' and q refer to the incident and scattered lepton, the incoming and outgoing proton or excited state Y and the exchanged photon, respectively. The elasticity z of the meson production process is defined as $z = (p \cdot p_\psi)/(p \cdot q)$ where p_ψ denotes the four-momentum of the produced vector meson. In the proton rest frame, z describes the fractional photon energy transferred to the vector meson. It is related to M_Y by $z \simeq 1 - (M_Y^2 - m_p^2 - t)/W_{\gamma p}^2$. For elastic events at low $|t|$, in which the proton stays intact, $z \simeq 1$.

In the photoproduction domain, i.e. at $Q^2 \rightarrow 0$, the incoming lepton is scattered at small angles and below $Q^2 \sim 1 \text{ GeV}^2$ it is not observed in the central detector. In the limit of photoproduction $W_{\gamma p}^2 = (p + q)^2$ is given by ys where $y = (E - p_z)_\psi/(2E_e)$. Here E and p_z denote the total energy and momentum component of the vector meson parallel to the proton beam direction¹ of the vector meson and E_e is the energy of the incident beam lepton. For the measurement of the elasticity the relation $z \simeq (E - p_z)_\psi/\Sigma(E - p_z)$ is used where $\Sigma(E - p_z)$ includes all measured final state particles. The variable t is approximated by the negative transverse momentum squared of the vector meson, i.e. $t \simeq -p_{t,\psi}^2$.

2.2 Detector and Data Selection

The H1 Detector is described in detail elsewhere [16]. For this analysis the central and forward tracking detectors, consisting of a system of drift and proportional chambers with a polar angular coverage between 7° and 165° , are used for the detection of charged decay particles. In addition the main and backward calorimeters, covering the polar angular regions $4^\circ - 153^\circ$ and $153^\circ - 177.5^\circ$, respectively, are used for lepton identification and for the determination of the event kinematics [16, 17]. The instrumented iron return yoke of the solenoidal magnet ($4^\circ < \theta < 171^\circ$) which surrounds the central H1 detector supplements the calorimeters in the identification of muons. Triggers based on lepton and track signatures are used to collect the events.

The analysis presented here is based on data corresponding to an integrated luminosity of 77 pb^{-1} . The data were taken in the years 1996 to 2000. Until 1997 HERA was operated with positrons of energy 27.5 GeV and protons of 820 GeV, while afterwards the proton energy was 920 GeV and both electrons and positrons were used. Events from $\psi(2S)$ and J/ψ production are selected using the direct decays into two leptons $\mu^+\mu^-$ or e^+e^- and the $\psi(2S)$ is also reconstructed via the cascade into a J/ψ and two charged pions with subsequent decay of the J/ψ into two leptons. The data selection resembles closely the procedure used in [3, 12]. Events with a scattered lepton candidate detected in the calorimeters with an energy deposit of more than 8 GeV are rejected. The accepted photoproduction event sample covers the range $Q^2 \lesssim 1 \text{ GeV}^2$ with an average $\langle Q^2 \rangle \sim 0.055 \text{ GeV}^2$ as determined from the Monte Carlo simulation.

¹The coordinate system of H1 defines the positive z -axis to be in the direction of the proton beam. The polar angle θ is then defined with respect to this axis.

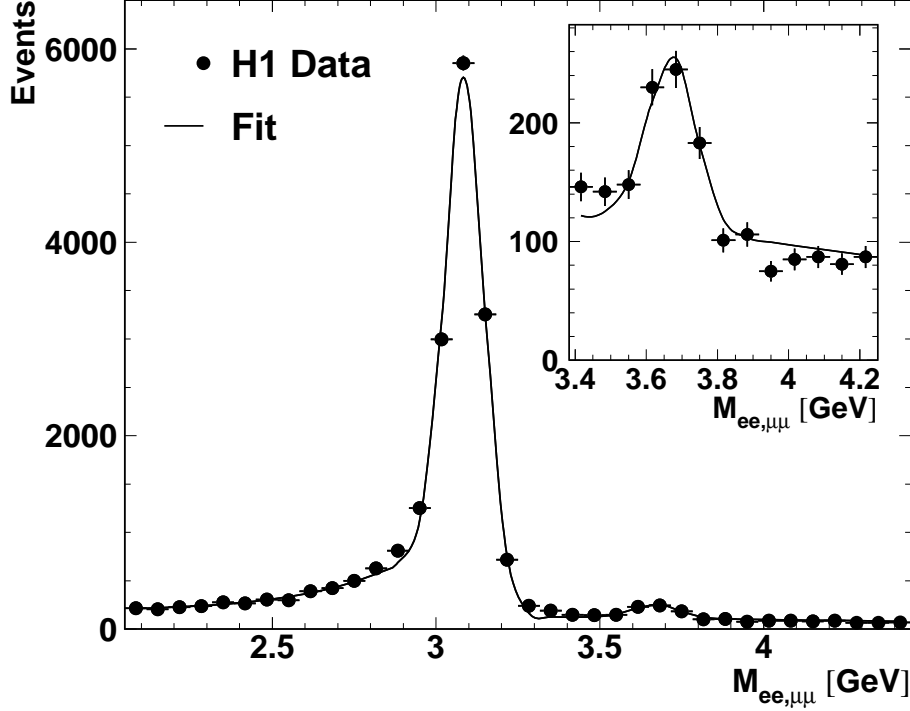


Figure 1: Mass spectrum ($|t| > 0.07 \text{ GeV}^2$) for the direct decay channel into leptons ($\mu^+\mu^-$ and e^+e^-) after the final selection. The insert shows the mass distribution restricted to the $\psi(2S)$ region. The curve shows the result of a fit combining Gaussian distributions for the J/ψ and $\psi(2S)$ signals, an exponential parametrisation of the radiative tail in the electron decay channel for the J/ψ and a linear background.

Vector meson decays into lepton pairs are selected by requiring exactly two tracks in the central tracking chambers, each with a transverse momentum greater than 0.8 GeV in a polar angular range² of $20^\circ < \theta < 160^\circ$. The tracks must define an event vertex in the ep interaction region. Both tracks are required to satisfy lepton identification requirements. The decay electrons are identified using the electromagnetic section of the calorimeters and energy loss dE/dx in the tracking chambers. Muons are identified in the instrumented iron return yoke or as minimum ionizing particles in the main calorimeter. Cosmic ray muon events are rejected using a track acollinearity requirement. For the selection of $\psi(2S)$ events via the cascade decay, $\psi(2S) \rightarrow (J/\psi \rightarrow \ell^+\ell^-)\pi^+\pi^-$, events with exactly four tracks are selected. In addition to two lepton candidate tracks, which are identified as described above, exactly two further central tracks with opposite charge are required, each with a transverse momentum of at least 0.12 GeV . The invariant mass of the two leptons is restricted to $2.4 (2.9) < M_{\ell\ell} < 3.3 \text{ GeV}$ for cascade decays with $J/\psi \rightarrow e^+e^-$ ($J/\psi \rightarrow \mu^+\mu^-$), respectively.

For the selection of the final diffractive (i.e. the sum of elastic and proton dissociative) event samples, further requirements are applied which ensure that the detector is essentially “empty” apart from the J/ψ and $\psi(2S)$ decay products. These requirements and the method used to separate the elastic and proton dissociative contributions are discussed in detail in section 2.4. Figure 1 shows the di-lepton mass distribution for the diffractive sample in the mass region of

²For the data sample recorded in the year 2000, the polar angle of the decay electrons was required to be in the range $30^\circ < \theta < 150^\circ$.

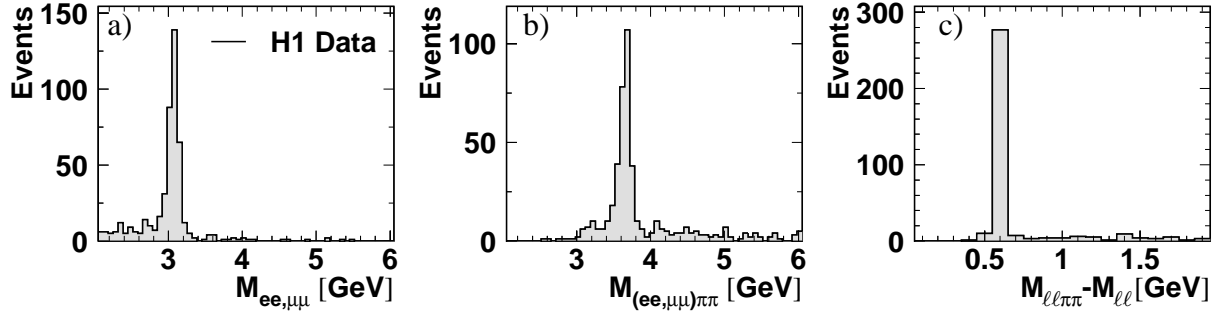


Figure 2: Mass spectra for the selected $\ell\ell\pi\pi$ sample; a) and b) show the $\ell\ell$ and $\ell\ell\pi\pi$ invariant mass distributions; c) shows the mass difference $M_{\ell\ell\pi\pi} - M_{\ell\ell}$ when selecting the $\ell\ell$ pairs reconstructed in the J/ψ mass window.

the J/ψ and $\psi(2S)$ mesons. The insert shows the same mass distribution restricted to the $\psi(2S)$ region revealing a clear signal of 307 ± 27 events above the non-resonant background. In decays with electrons the signals have a tail to lower masses due to the presence of radiative decays and radiation in the material of the detector. The non-resonant background is dominated by the process $\gamma\gamma \rightarrow \ell^+\ell^-$ in which the two photons couple to the beam lepton and to the proton, respectively. For the direct decays of $\psi(2S)$ mesons the non-resonant background fraction is large. It is smaller for the $J/\psi \rightarrow \ell^+\ell^-$ events and for the cascade decays of $\psi(2S)$ mesons. Figure 2a and b show the $\ell\ell$ and $\ell\ell\pi\pi$ mass distributions for the 4-prong sample. In Fig. 2c the mass difference $M_{\ell\ell\pi\pi} - M_{\ell\ell}$ is shown. A signal of 278 events in the range $|M_{\ell\ell\pi\pi} - M_{\ell\ell} - 0.59 \text{ GeV}| < 0.06 \text{ GeV}$ is seen with negligible background.

2.3 Monte Carlo Models and Acceptances

The acceptances and efficiencies for triggering, track reconstruction, event selection and lepton identification are calculated using Monte Carlo simulations. The J/ψ and $\psi(2S)$ samples are generated using the program DIFFVM [18] and are passed through a detailed simulation of the detector response based on the GEANT program [19] and the same reconstruction software as was used for the data. DIFFVM generates events according to the cross section dependences $d\sigma/dt \propto W_{\gamma p}^{4\epsilon} e^{bt}$ for elastic photoproduction of charmonium. For production with proton dissociation $d^2\sigma/dtdM_Y^2 \propto W_{\gamma p}^{4\epsilon} e^{b't} M_Y^\beta$ is used. The parameters were chosen such that the main features of J/ψ and $\psi(2S)$ production are described: $b = 4.8 \text{ GeV}^{-2}$; $b' = 1.6 \text{ GeV}^{-2}$; $\beta = -2.16$ and $4\epsilon = 0.96$. Possible deviations from these parametrisations are taken into account in the systematic error analysis. The decay angular distributions of charmonium decaying directly into two leptons are simulated assuming s -channel helicity conservation. For background estimation the generators LPAIR [20] and GRAPE [21] are used, which simulate the process $\gamma\gamma \rightarrow \ell^+\ell^-$. The contributions of radiative decays to J/ψ or $\psi(2S) \rightarrow e^+e^-$ are estimated with the generator PHOTOS [22].

Detailed comparisons between the simulation and the data are facilitated by the large J/ψ data sample in which the background fraction is small. Figure 3 shows the transverse momentum and polar angular distributions of the tracks in the direct decays of J/ψ into muons and electrons both for data and simulation. There is good agreement. Figure 4 shows that the simulation

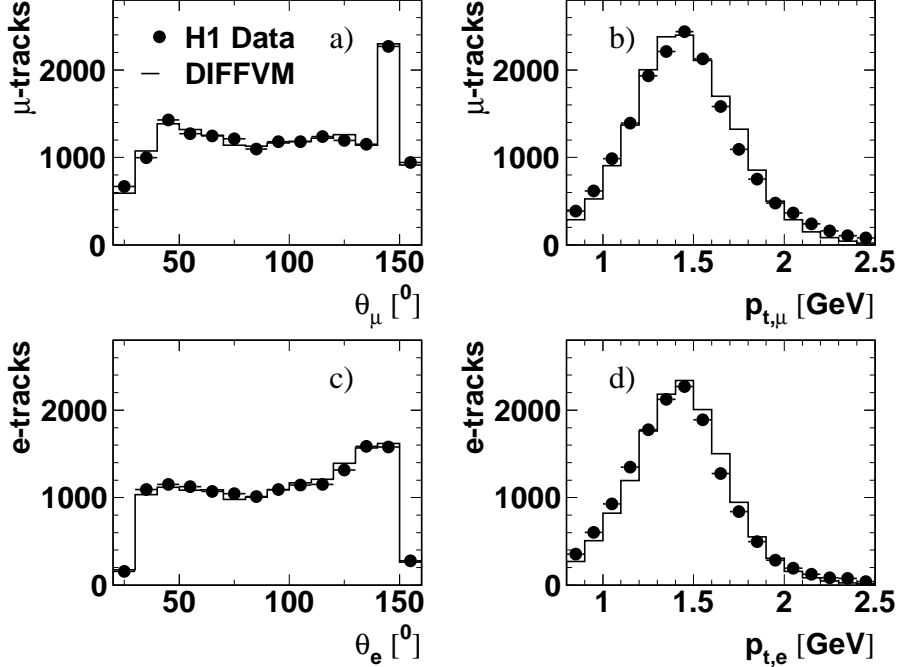


Figure 3: Distributions for the decays of J/ψ mesons into muons (a,b) and electrons (c,d). The polar angles (a,c) and the transverse momenta (b,d) of the decay leptons are shown for the data (points) and the DIFFVM Monte Carlo simulation (histograms). The Monte Carlo simulation is normalised to the number of events in the data.

for the cascade decays of $\psi(2S)$ adequately describes the data. The simulation generates a flat $\pi\pi$ -mass distribution in the available phase space, ignoring the dependence arising from the matrix element. To correct for this the simulation was reweighted using an event weight $\propto (M_{\pi\pi}^2 - 4m_\pi^2)^2$ as determined in [23]. This results in a good description of the $M_{\pi\pi}$ spectrum (Fig. 4e).

The detector simulation has been checked extensively and separately for each data taking period and decay lepton type using independent data samples and was adjusted where necessary. Typical trigger efficiencies are 45% for the muon channel and 55% for the electron channel. The efficiency for identifying a muon (electron) is typically 75% (85%). Together with the geometric detector acceptance the overall efficiency varies between 5 and 10% with $W_{\gamma p}$. In the range studied here the variation of the overall efficiency with $|t|$ is small. The resolution in t for the muon decay channel is typically 0.035 GeV^2 and increases to 0.060 GeV^2 at $|t| = 1.2 \text{ GeV}^2$. For the electron decay channel the resolution is roughly 15% worse than this due to bremsstrahlung.

2.4 Separation of Elastic and Proton Dissociative Processes

For the analysis of the t -dependence it is necessary to separate elastic events from those with dissociation of the proton into a small mass system. To tag events with proton dissociation the forward section of the calorimeter ($\theta < 10^\circ$), the Proton Remnant Tagger ($0.06^\circ < \theta < 0.26^\circ$) and the Forward Muon Detector ($3^\circ < \theta < 17^\circ$) are used. With these forward detectors, dissociated proton states with masses $M_Y \gtrsim 1.6 \text{ GeV}$ can be tagged [24]. In the following, events with (without) signals in the forward detectors are called ‘tagged’ (‘untagged’), respectively.

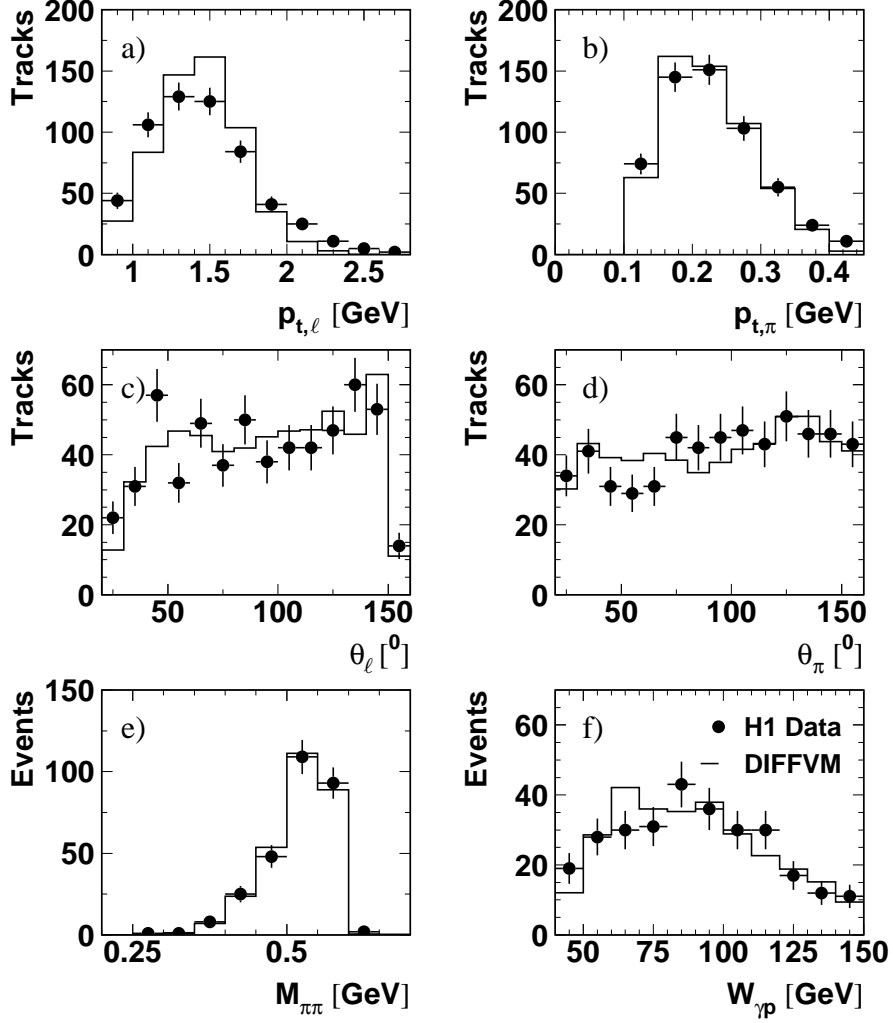


Figure 4: Distributions for the cascade decays of $\psi(2S)$ mesons: a) the transverse momentum of the decay leptons and b) the decay pions; c) the polar angle of the decay leptons and d) the decay pions; e) the two-pion invariant mass and f) the photon proton center-of-mass energy $W_{\gamma p}$. The points show the data. The histograms show the DIFFVM Monte Carlo simulation normalised to the number of events in the data after event reweighting (see text).

In the ‘untagged’ sample no additional tracks other than those from the J/ψ or $\psi(2S)$ decay products are allowed. In the ‘tagged’ sample at most one additional track measured in the forward tracking chambers in the polar angular region below 10° is allowed and an elasticity $z > 0.95$ is required in order to ensure that the event sample is diffractive.

The elastic and proton dissociative contributions to the diffractive sample are extracted from the untagged and tagged event samples respectively, taking the background admixtures from proton dissociative events in the untagged sample ($\sim 15\%$) and elastic events in the tagged sample ($\sim 10\%$) into account. The admixtures are due to the limited angular coverage of the forward detectors, their inefficiencies and noise fluctuations.

In Table 1 the estimated relative signal and background contributions are listed for the tagged and untagged samples of the different decay channels. The non-resonant background in the

	$\psi(2S) \rightarrow \ell\ell$		$\psi(2S) \rightarrow \ell\ell\pi\pi$		$J/\psi \rightarrow \ell\ell$	
	untagged	tagged	untagged	tagged	untagged	tagged
Elastic	39%	6%	85%	10%	80%	9%
Proton Dissociative	6%	54%	15%	90%	14%	85%
Non-resonant Bg.	55%	40%	–	–	6%	6%

Table 1: Estimated contributions to the tagged and untagged samples for the three different charmonium decays and the non-resonant backgrounds (see text).

mass window of ± 150 MeV around the nominal charmonium masses is determined from the side-band events. It is found to be negligible for the $\psi(2S)$ cascade decay samples. The elastic and proton dissociative contributions in Table 1 are determined using a Monte Carlo simulation of the forward region of the detector and the beamline. In the simulation the relative contributions from the proton dissociative and elastic channels are adjusted to reproduce the distributions measured in the forward detectors. The uncertainty on the determination of the admixtures is evaluated by variation of the simulated forward detector efficiencies and of the simulated cross section dependence on the mass M_Y of the dissociated proton system [25]. The resulting uncertainty on the final cross sections is 6%. Within experimental errors, equal cross sections for elastic and proton dissociative photoproduction of charmonium are found for the measured M_Y and t regions, which is in agreement with previous results [1, 3, 12].

The fraction of erroneously tagged events in the elastic sample increases with $|t|$ and, with the present analysis method, no distinction between elastic and proton dissociative events can be made for $|t| \gtrsim 1 \text{ GeV}^2$. However, since the t -dependence of the elastic channel is much steeper than that for proton dissociation, the elastic contribution at $|t| \gtrsim 1 \text{ GeV}^2$ can safely be neglected.

2.5 $\psi(2S)$ and J/ψ Signal Determination

For the measurement of the $W_{\gamma p}$ dependence the numbers of signal events are determined for the diffractive samples in four bins of $W_{\gamma p}$. For events with direct decays into muons a simultaneous fit is used in which the $\psi(2S)$ or J/ψ signals are parametrised by Gaussian distributions and the non-resonant background follows a linear dependence. In an alternative method the non-resonant background is estimated using the generator LPAIR [20] and is subtracted from the number of signal events, counted in mass windows of ± 150 MeV width around the nominal J/ψ and $\psi(2S)$ masses. For the number of J/ψ signal events agreement within 2% between the two methods is found. For the direct $\psi(2S)$ decays into muons the number of signal events obtained from the fits differs by up to 10% from that obtained when using LPAIR to describe the background. These differences are taken as systematic errors.

For the direct decays of $\psi(2S)$ and J/ψ into electrons the number of signal events is determined using a fit to the mass spectrum with Gaussians for the J/ψ and $\psi(2S)$ signals, an exponential distribution for the radiative tails and a linear dependence for the non-resonant background. The systematic error in this method is estimated by comparing the result for the non-resonant background with that of the Monte Carlo generator GRAPE [21]. For J/ψ decays into electrons

the resulting systematic error is 5%. For the direct $\psi(2S)$ decays into electrons the uncertainty on the signal determination is estimated to be 15%, which is larger than that for J/ψ due to the larger background fraction.

For the cascade decays the non-resonant background is very small and all events found in the range $|M_{\ell\ell\pi\pi} - M_{\ell\ell} - 0.59 \text{ GeV}| < 0.06 \text{ GeV}$ are assigned to the signal (see Fig. 2c). The number of J/ψ events is corrected for the fraction of $\psi(2S)$ events with decays into a J/ψ and neutral particles. This correction is estimated to be $(3.4 \pm 0.9)\%$ based on the results of this analysis (see below). The contribution to the $\psi(2S)$ sample from decays of $\psi(3S)$ and higher excited states is expected to be small and is neglected.

3 Results

The results are given for an average $\langle Q^2 \rangle \sim 0.055 \text{ GeV}^2$ and cover an energy range $40 < W_{\gamma p} < 150 \text{ GeV}$. For the proton dissociative channel the kinematic region is restricted to $|t| < 5 \text{ GeV}^2$ and $(M_Y/W_{\gamma p})^2 < 0.05$.

3.1 Energy Dependence of $\sigma(\psi(2S))/\sigma(J/\psi)$

The ratio of $\psi(2S)$ to J/ψ cross sections $R = \sigma(\psi(2S))/\sigma(J/\psi)$ is measured as a function of $W_{\gamma p}$. The total diffractive $\psi(2S)$ and J/ψ samples, i.e. the sum of the tagged and the untagged samples as defined in section 2.4, are used in order to minimise the systematic and statistical errors. The experimental signatures of the leptonic decay channels of $\psi(2S)$ and J/ψ mesons are very similar and the large sample of J/ψ mesons has been used to support the study of the experimental systematics for the $\psi(2S)$ measurement. In the context of this analysis a complete measurement of the J/ψ cross section was performed [25], yielding a $W_{\gamma p}$ dependence which is consistent with the results of our earlier publication [3].

The cross section ratio is obtained by taking the ratio of the corrected numbers of $\psi(2S)$ events to the corrected number of J/ψ events in each $\psi(2S)$ decay channel separately. Each of the samples is corrected for its specific trigger efficiency, event selection efficiency and the $\psi(2S)$ and J/ψ branching ratios³. In the evaluation of the systematic error on the cross section ratio the errors on the integrated luminosity, the trigger efficiency, the lepton identification and track reconstruction efficiencies and the detector acceptance are found to be highly correlated between the J/ψ and the $\psi(2S)$ samples and therefore largely cancel. The remaining errors from these sources amount to 5% in total. For the direct decays the uncertainty in the determination of the number of $\psi(2S)$ signal events is the dominant systematic error contributing 10% for decays to $\mu^+\mu^-$ and 15% for decays to e^+e^- (see section 2.5). For the cascade decays the uncertainty in the pion track reconstruction efficiency of 12% dominates the systematic error.

Figure 5 and Table 2 show the measured cross section ratio as a function of $W_{\gamma p}$. In the figure the inner error bars reflect the statistical errors, the outer error bars show the statistical and the

³The branching ratios for the $\psi(2S)$ are $(0.79 \pm 0.05)\%$, $(0.77 \pm 0.17)\%$ and $(34.8 \pm 2.8)\%$ for the decays to e^+e^- , $\mu^+\mu^-$ and $J/\psi\pi^+\pi^-$, respectively. For the J/ψ decays into muons and electrons the branching ratios are $(5.88 \pm 0.10)\%$ and $(5.93 \pm 0.10)\%$, respectively [26].

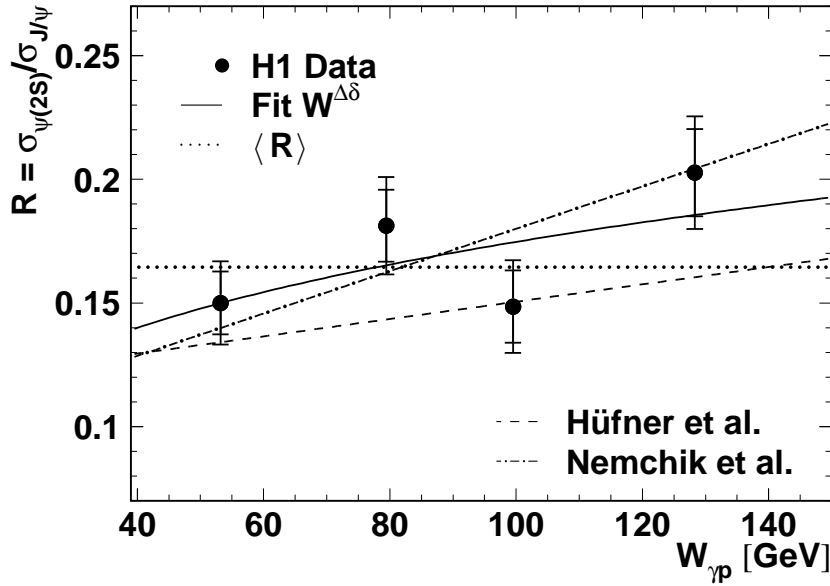


Figure 5: The ratio $R(W_{\gamma p}) = \sigma_{\psi(2S)}/\sigma_{J/\psi}$ for events with $z > 0.95$. The inner error bars show the statistical error. The outer error bars show the statistical and systematic errors added in quadrature. An additional normalisation uncertainty of 0.007 due to the errors on the branching ratios is not shown. A fit $R \propto (W_{\gamma p}/90 \text{ GeV})^{\Delta\delta}$ with a value for $\Delta\delta$ of 0.24 (solid line) and predictions from [9] (dashed-dotted line) and [10] (dashed line) are also shown.

systematic errors added in quadrature, excluding the uncertainty from the branching ratios. The overall ratio, shown in Fig. 5 as a dotted line, yields the value

$$R = 0.166 \pm 0.007(\text{stat.}) \pm 0.008(\text{sys.}) \pm 0.007(\text{BR}),$$

in good agreement with an earlier measurement [12]. This result is obtained by averaging over the ratios for the different decay channels and integrating over the four bins in $W_{\gamma p}$, taking proper account of the correlations in the branching ratio errors. The solid line shows a fit of the form $R(W_{\gamma p}) \propto W_{\gamma p}^{\Delta\delta}$ to the data points yielding a value of $\Delta\delta = 0.24 \pm 0.17$ with $\chi^2 = 3.1$ for 2 degrees of freedom, where the error includes systematic and statistical uncertainties added in quadrature. The energy dependence of the diffractive $\psi(2S)$ photoproduction cross section is thus similar or possibly slightly steeper than that for J/ψ mesons. The calculations of [9] and of [10]⁴ which are valid for elastic photoproduction are also shown. Both groups predict a somewhat steeper energy dependence for the $\psi(2S)$ than for the J/ψ meson, compatible with the data in both slope and normalisation.

3.2 t -Dependences of the Elastic and Proton Dissociative Channels

In order to study the t -dependences, the data are divided into the tagged and untagged samples as described in section 2.4. Figure 6 shows the normalised differential cross sections $1/\sigma \cdot d\sigma/dt$ for events in mass windows of $\pm 150 \text{ MeV}$ around the nominal J/ψ and $\psi(2S)$ masses for each

⁴The different parametrisations given in [10] vary considerably in normalisation. In Fig. 5 the parametrisation referred to in [10] as ‘GBW(BT)’ is shown.

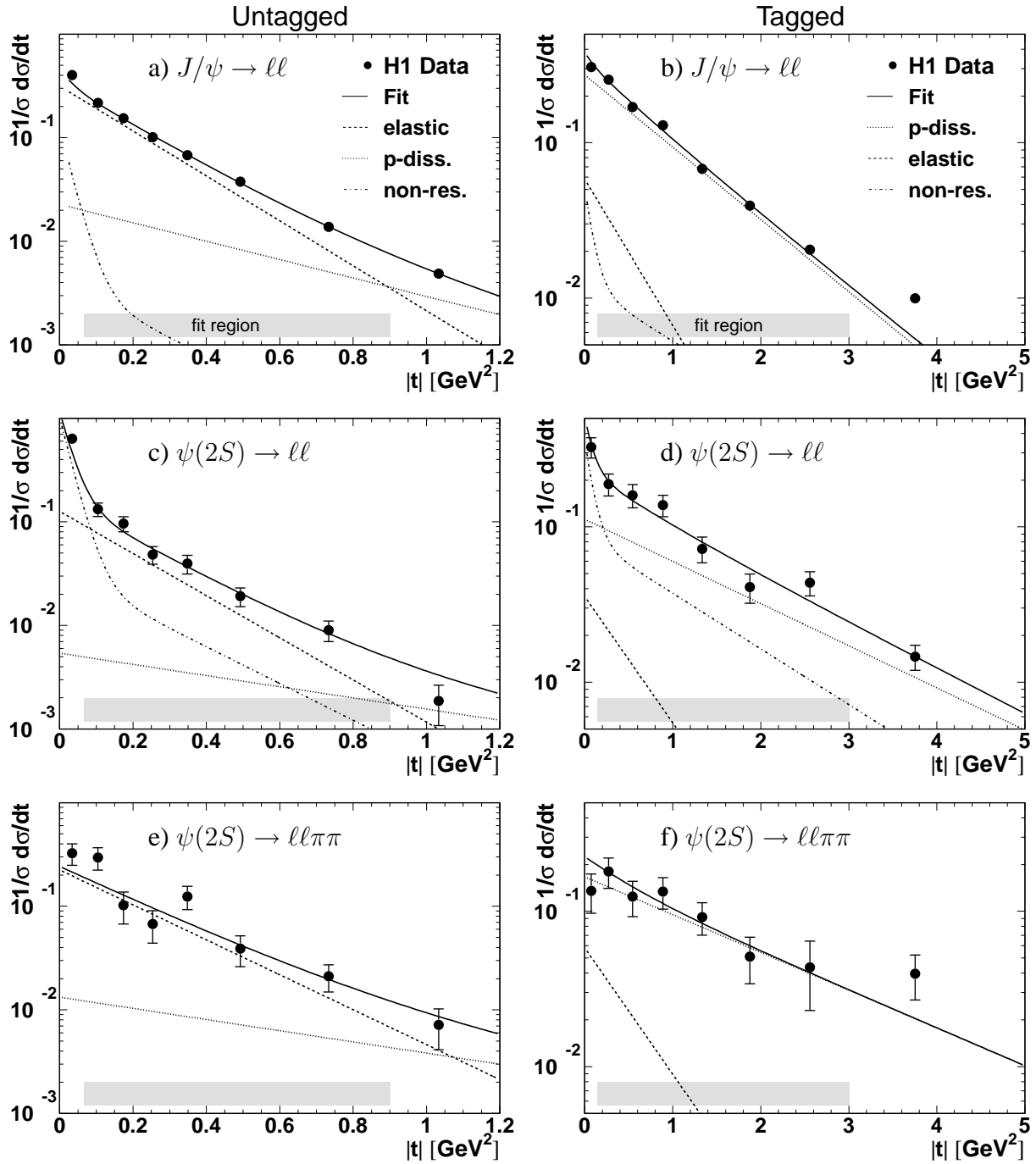


Figure 6: Normalised differential cross sections $1/\sigma \cdot d\sigma/dt$ as a function of $|t|$ for events a) in the J/ψ mass window without a signal in the forward detectors (untagged), b) in the J/ψ mass window with a signal in the forward detectors (tagged), c) untagged and d) tagged events in the $\psi(2S)$ mass window for direct decays to lepton pairs, e) untagged and f) tagged $\psi(2S)$ events with cascade decays. The solid lines show the results of the fits described in the text. The dashed (dotted) curves show the contributions from the elastic (proton dissociative) processes, respectively. For the direct decays into leptons (a-d) the contributions from the non-resonant background (dashed-dotted curves) are also shown. The shaded bands indicate the fit regions.

of the three samples J/ψ , $\psi(2S)$ with direct and $\psi(2S)$ with cascade decays. The data samples consist of events with decays into both muons and electrons and are corrected for efficiencies but not for remaining backgrounds. The untagged (tagged) cross sections are displayed in the left (right) column of the figure. The main contribution to the untagged cross section is from the elastic diffractive process with contaminations from the untagged proton dissociative process and from non-resonant background. The main contribution to the tagged cross section is from the proton dissociative process, with contaminations from the non-resonant background and from the elastic process.

The method used to analyse the t -dependence is optimised for samples with large non-resonant background, i.e. the direct $\psi(2S)$ decays. The same method is used for the analysis of the t -dependences of the J/ψ samples and the $\psi(2S)$ samples with cascade decays, for consistency. The t -dependences of the elastic and the proton dissociative contributions are described by single exponential distributions e^{bt} . The slope parameters b are extracted using an iterative procedure of combined fits to the tagged and untagged samples. The non-resonant backgrounds are described by sums of two exponential functions. The t -dependence and relative normalisation of the non-resonant background are determined from an analysis of the side-band events in the range $4 < M_{\ell\ell} < 8$ GeV, and are fixed in the fit procedure. The observed behaviour is reproduced by the LPAIR and GRAPE generators.

In the iteration procedure the relative fractions of the background contributions are fixed to the numbers given in section 2.4. In the first step a fit is performed for the proton dissociative slope parameter in the tagged sample, neglecting the elastic contamination. This estimate is then used to compute the proton dissociative contamination in the untagged sample. The Monte Carlo simulation is used in this calculation to account for the t -dependence of the probability of failing to tag proton dissociation events. Secondly, a fit to the untagged sample is performed to extract the slope parameter of the elastic channel, correcting for the untagged proton dissociative contribution. This measurement of the elastic channel is then used to estimate the elastic contribution in the tagged sample and to improve the measurement of the proton dissociative process obtained in the first step. The fit procedure converges after one iteration since the elastic contamination in the tagged sample is small (see Fig. 6). The elastic slope parameters b_{el} are extracted for each of the three untagged samples in the region of $0.07 < |t| < 0.9$ GeV² excluding the regions with large non-resonant background (lowest $|t|$ bin) or large contribution from proton dissociation (highest $|t|$ bin). Similarly, the proton dissociative slope parameters b_{pd} are extracted from the tagged samples in the region of $0.15 < |t| < 3$ GeV². The lowest $|t|$ bin is excluded since for proton dissociation, the minimum kinematically allowed value of $|t|$ can be large for large masses M_Y . The highest $|t|$ bin is excluded because at large values of $|t| \gtrsim 3$ GeV², the data deviate from an exponential behaviour. In Fig. 6 the solid lines indicate the parametrisations of the data as obtained from the fits, including the contributions from the signals and the backgrounds.

The systematic uncertainty on the b values is estimated by varying the selection cuts and trigger conditions, the $|t|$ -dependences of the efficiencies and acceptances and the admixtures of the background contributions (both relative normalisations and shapes) resulting in the uncertainties given in Table 3. The dominant error source for the elastic slope parameter is the proton dissociative background. For the proton dissociative slope parameter the t -dependences of the trigger and event selection efficiencies are the dominant error sources.

From the untagged samples the fits yield the elastic slope parameters $b_{el}^{\psi(2S)} = (4.31 \pm 0.57 \pm 0.46) \text{ GeV}^{-2}$ for the $\psi(2S)$ and $b_{el}^{J/\psi} = (4.99 \pm 0.13 \pm 0.39) \text{ GeV}^{-2}$ for the J/ψ , where the first error is statistical and the second error describes the systematic uncertainties. The result for $b_{el}^{J/\psi}$ confirms the previous measurement [3]. From the tagged samples the proton dissociative parameters $b_{pd}^{\psi(2S)} = (0.59 \pm 0.13 \pm 0.12) \text{ GeV}^{-2}$ for the $\psi(2S)$ and $b_{pd}^{J/\psi} = (1.07 \pm 0.03 \pm 0.11) \text{ GeV}^{-2}$ for the J/ψ are obtained. These results are listed in Table 4, together with the results for separate fits to the samples with muons or with electrons alone and to the samples with direct and cascade $\psi(2S)$ decays. Good agreement is observed between the results from the different samples.

The measured slope parameters b_{pd} with proton dissociation are considerably smaller than in the elastic case. This is in agreement with expectations [15]. The t -dependence of elastic $\psi(2S)$ photoproduction is similar to that of J/ψ . This is in agreement with expectations in the additive quark model [15] and also within the colour dipole model [9]. For proton dissociation a somewhat shallower t -dependence is measured for the $\psi(2S)$ than for the J/ψ . The difference between the proton dissociative slope parameters of J/ψ and $\psi(2S)$ mesons amounts to 2.3 standard deviations and can be interpreted as an effect of the $\psi(2S)$ wavefunction node on the t -dependence. In proton dissociation this is more visible than in the elastic process due to the lower overall values of the slope parameter b_{pd} .

4 Summary

The $W_{\gamma p}$ and t -dependences of diffractive $\psi(2S)$ photoproduction have been measured for the first time. For the total diffractive cross section ratio $R = \sigma_{\psi(2S)}/\sigma_{J/\psi}$ a value of

$$R = 0.166 \pm 0.007(stat.) \pm 0.008(sys.) \pm 0.007(BR)$$

is obtained in the region $40 < W_{\gamma p} < 150 \text{ GeV}$ and $Q^2 < 1 \text{ GeV}^2$ consistent with and improving the errors of our previous measurement [12]. The cross section ratio has been measured in four bins of $W_{\gamma p}$ and the result indicates that the energy dependence of $\psi(2S)$ photoproduction is similar or possibly somewhat steeper than that of J/ψ production. The data are well described by pQCD calculations [9, 10].

The t -dependences of elastic and proton dissociative charmonium production have been measured. The t -dependence of elastic $\psi(2S)$ meson production is compatible with an exponential behaviour $\propto e^{bt}$ in the measured range of $|t| < 0.9 \text{ GeV}^2$, with $b_{el}^{\psi(2S)} = (4.31 \pm 0.57 \pm 0.46) \text{ GeV}^{-2}$. This value is similar to the result for J/ψ mesons, $b_{el}^{J/\psi} = (4.99 \pm 0.13 \pm 0.39) \text{ GeV}^{-2}$ and thus confirms the predictions of [9, 10]. The proton dissociative slope parameter has been determined to be $b_{pd}^{\psi(2S)} = (0.59 \pm 0.13 \pm 0.12) \text{ GeV}^{-2}$ for the $\psi(2S)$ meson, somewhat smaller than that for the J/ψ meson, which is measured to be $b_{pd}^{J/\psi} = (1.07 \pm 0.03 \pm 0.11) \text{ GeV}^{-2}$. These results are well described by pQCD calculations which take into account the differences in the wavefunctions of the J/ψ and its radial excitation.

Acknowledgments

We are grateful to the HERA machine group whose outstanding efforts have made and continue to make this experiment possible. We thank the engineers and technicians for their work in constructing and now maintaining the H1 detector, our funding agencies for financial support, the DESY technical staff for continual assistance and the DESY directorate for the hospitality which they extend to the non DESY members of the collaboration.

$W_{\gamma p}$ Interval [GeV]	$\langle W_{\gamma p} \rangle$ [GeV]	$R(W_{\gamma p})$
40 – 70	53.2	$0.150 \pm 0.013 \pm 0.011$
70 – 90	79.4	$0.181 \pm 0.015 \pm 0.013$
90 – 110	99.5	$0.149 \pm 0.015 \pm 0.012$
110 – 150	128.3	$0.203 \pm 0.018 \pm 0.014$

Table 2: Results for the $\psi(2S)$ to J/ψ photoproduction cross section ratio $R = \sigma_{\psi(2S)}/\sigma_{J/\psi}$ in four bins of $W_{\gamma p}$ together with the statistical and systematic errors. An additional normalisation uncertainty of 0.007 due to the branching ratios is not included in the errors.

Systematic errors [GeV ⁻²]	$\psi(2S) \rightarrow \ell\ell$		$\psi(2S) \rightarrow \ell\ell\pi\pi$		$J/\psi \rightarrow \ell\ell$	
	Δb_{el}	Δb_{pd}	Δb_{el}	Δb_{pd}	Δb_{el}	Δb_{pd}
Trigger and selection efficiencies	0.2	0.1	0.2	0.1	0.2	0.1
t -dependence of forward tagging	0.2	0.03	0.2	0.03	0.2	0.03
Normalisation of non-res. background	0.11	0.01	–	–	–	–
t -dependence of non-res. background	0.05	0.04	–	–	–	–
Normalisation of p -diss.(elas.) background	0.35	0.01	0.35	0.01	0.27	0.01
t -dependence of p -diss.(elas.) background	0.06	0.05	0.06	0.05	0.03	0.03
Total error	0.47	0.12	0.45	0.12	0.39	0.11

Table 3: Table of systematic errors (in GeV⁻²) in the determination of the elastic and proton dissociative slope parameters b of $\psi(2S)$ production with direct and cascade decays and J/ψ production.

	b_{el} [GeV ⁻²]	b_{pd} [GeV ⁻²]
$\psi(2S) \rightarrow \mu\mu$	4.76 ± 0.78	0.69 ± 0.22
$\psi(2S) \rightarrow ee$	3.51 ± 2.44	0.42 ± 0.35
$\psi(2S) \rightarrow \mu\mu\pi^+\pi^-$	3.19 ± 0.96	0.53 ± 0.28
$\psi(2S) \rightarrow ee\pi^+\pi^-$	5.91 ± 2.74	0.57 ± 0.26
$J/\psi \rightarrow \mu\mu$	4.98 ± 0.15	1.10 ± 0.04
$J/\psi \rightarrow ee$	5.05 ± 0.25	1.01 ± 0.04
$\psi(2S) \rightarrow \ell\ell$	$4.69 \pm 0.73 \pm 0.45$	$0.62 \pm 0.18 \pm 0.12$
$\psi(2S) \rightarrow \ell\ell\pi^+\pi^-$	$3.88 \pm 0.92 \pm 0.47$	$0.56 \pm 0.19 \pm 0.12$
$\psi(2S)$	$4.31 \pm 0.57 \pm 0.46$	$0.59 \pm 0.13 \pm 0.12$
J/ψ	$4.99 \pm 0.13 \pm 0.39$	$1.07 \pm 0.03 \pm 0.11$

Table 4: Slope parameters for charmonium production for the elastic (left column) and proton dissociative (right column) component. For the separate electron and muon channels only the statistical errors are given. For the results combining both channels, both statistical and systematic errors are quoted.

References

- [1] S. Aid *et al.* [H1 Collaboration], Nucl. Phys. B **472**, (1996) 3 [hep-ex/9603005].
- [2] J. Breitweg *et al.* [ZEUS Collaboration], Z. Phys. C **75**, (1997) 215 [hep-ex/9704013].
- [3] C. Adloff *et al.* [H1 Collaboration], Phys. Lett. B **483**, (2000) 23 [hep-ex/0003020].
- [4] S. Chekanov *et al.* [ZEUS Collaboration], “Exclusive photoproduction of J/psi mesons at HERA”, arXiv:hep-ex/0201043.
- [5] A. D. Martin, M. G. Ryskin and T. Teubner, Phys. Rev. D **62**, (2000) 014022 [hep-ph/9912551].
- [6] L. Frankfurt, M. McDermott and M. Strikman, JHEP **0103**, 045 (2001) [hep-ph/0009086].
- [7] B. Z. Kopeliovich and B. G. Zakharov, Phys. Rev. D **44** (1991) 3466.
- [8] B. Z. Kopeliovich, J. Nemchik, N. N. Nikolaev and B. G. Zakharov, Phys. Lett. B **309** (1993) 179 [hep-ph/9305225].
- [9] J. Nemchik, N. N. Nikolaev, E. Predazzi, B. G. Zakharov and V. R. Zoller, J. Exp. Theor. Phys. **86**, (1998) 1054. [Zh. Eksp. Teor. Fiz. **113**, (1998) 1930] [hep-ph/9712469].
- [10] J. Hüfner, Yu.P. Ivanov, B. Z. Kopeliovich and A. V. Tarasov, Phys. Rev. D **62** (2000) 094022 [hep-ph/0007111].
- [11] P. Hoyer and S. Peigne, Phys. Rev. D **61** (2000) 031501.
- [12] C. Adloff *et al.* [H1 Collaboration], Phys. Lett. B **421**, (1998) 385 [hep-ex/9711012].
- [13] M. Derrick *et al.* [ZEUS Collaboration], Z. Phys. C **69**, (1995) 39 [hep-ex/9507011].
- [14] S. Aid *et al.* [H1 Collaboration], Nucl. Phys. B **463** (1996) 3 [hep-ex/9601004].
- [15] M. G. Ryskin, Y. M. Shabelski and A. G. Shuvaev, Phys. Lett. B **446** (1999) 48 [hep-ph/9803434].
- [16] I. Abt *et al.* [H1 Collaboration], Nucl. Instrum. Meth. A **386**, (1997) 310 and 348.
- [17] T. Nicholls *et al.* [H1 SPACAL Group Collaboration], Nucl. Instrum. Meth. A **374**, (1996) 149.
- [18] B. List, A. Mastroberardino in: Proc. of the Workshop on Monte Carlo Generators for HERA Physics, DESY-PROC-1999-02 (1999) 396.
- [19] R. Brun, F. Bruyant, M. Maire, A. C. McPherson and P. Zancarini, CERN-DD/EE/84-1.
- [20] S. P. Baranov, O. Dünger, H. Shooshtari and J. A. Vermaseren, In *Hamburg 1991, Proceedings, Physics at HERA, vol. 3* 1478-1482. (see HIGH ENERGY PHYSICS INDEX 30 (1992) No. 12988).

- [21] T. Abe, Comput. Phys. Commun. **136**, (2001) 126 [hep-ph/0012029].
- [22] E. Barberio and Z. Was, Comput. Phys. Commun. **79**, (1994) 291.
- [23] T. N. Pham, B. Pire and T. N. Truong, Phys. Lett. B **61**, (1976) 183.
- [24] T. Ahmed *et al.* [H1 Collaboration], Phys. Lett. B **348** (1995) 681 [hep-ex/9503005].
- [25] D. Schmidt, Ph.D. Thesis, (2001) University of Hamburg, 155pp, in German (URL:http://www-h1.desy.de/publications/theses_list.html).
- [26] D. E. Groom *et al.* [Particle Data Group Collaboration], Eur. Phys. J. C **15**, (2000) 1 and 2001 partial update for edition 2002 (URL: <http://pdg.lbl.gov>)